MAGNETOTELLURIC SURVEYS
ALUM & SILVER PEAK, NEVADA - USA

Final Report: 3D Inversion Modeling

Volume 1 of 1

Prepared for

SIERRA GEOTHERMAL POWER

By

GEOSYSTEM

WesternGeco EM

Milan, Italy

Effective date: March 2010

Revision History:

Rev. No.	Effective Date	Description	Prepared by	Reviewed by	Approved by
01	09 March 2010	First draft	Alessandra Battaglini		
02	17 March 2010		Ersan Turkoglu	Gary McNeice	

CONTENTS

FIGURES

SUMMARY

Under contract from Sierra Geothermal Power, WesternGeco's Land EM group Geosystem carried out a total of 79 magnetotelluric (MT) soundings at Alum and 69 MT soundings at Silver Peak areas, Nevada.

3D MT resistivity inversion modelling was carried out separately for the sub-areas Alum and Silver Peak, to delineate the resistivity structure from surface to depths of 2.5km. Seventy-three (73) of the seventy-nine (79) MT soundings acquired in Alum survey, and all of the MT soundings acquired in the Silver Peak MT survey were used in the 3D inversion procedure.

The final 3D inversion models used 150x150m spacing for the horizontal directions (X and Y) for the both areas. The vertical mesh thickness was kept 15m and 10m throughout the topography for Alum and Silver Peak 3D mesh models respectively. The vertical mesh spacing was gradually increased by a factor of 1.1 for Alum and 1.05 for Silver Peak until the thickness reached 100m which was increased again after approximately 5km depth. 3D inversion was able to provide very good fit to the observed MT data and produced stable 3D resistivity models for both survey areas.

1 INTRODUCTION

Two MT surveys of respectively 79 and 69 stations were carried out at Alum and Silver Peak prospects, Nevada, USA.

MT stations were collected along seven NW-SE aligned profiles in the Alum survey area and along 10 E-W aligned profiles in the Silver Peak survey area (Figure 1, see also Plate 1 for a larger scale, and Figure 2 for detailed areas). Station distribution and the density of the sites form suitable conditions for 3D inversions for both of these areas.

Acquisition, operations and data processing details are given in the Operational Report (Geosystem, 2010), whilst MT data analysis and 3D inversion modelling results are presented here.

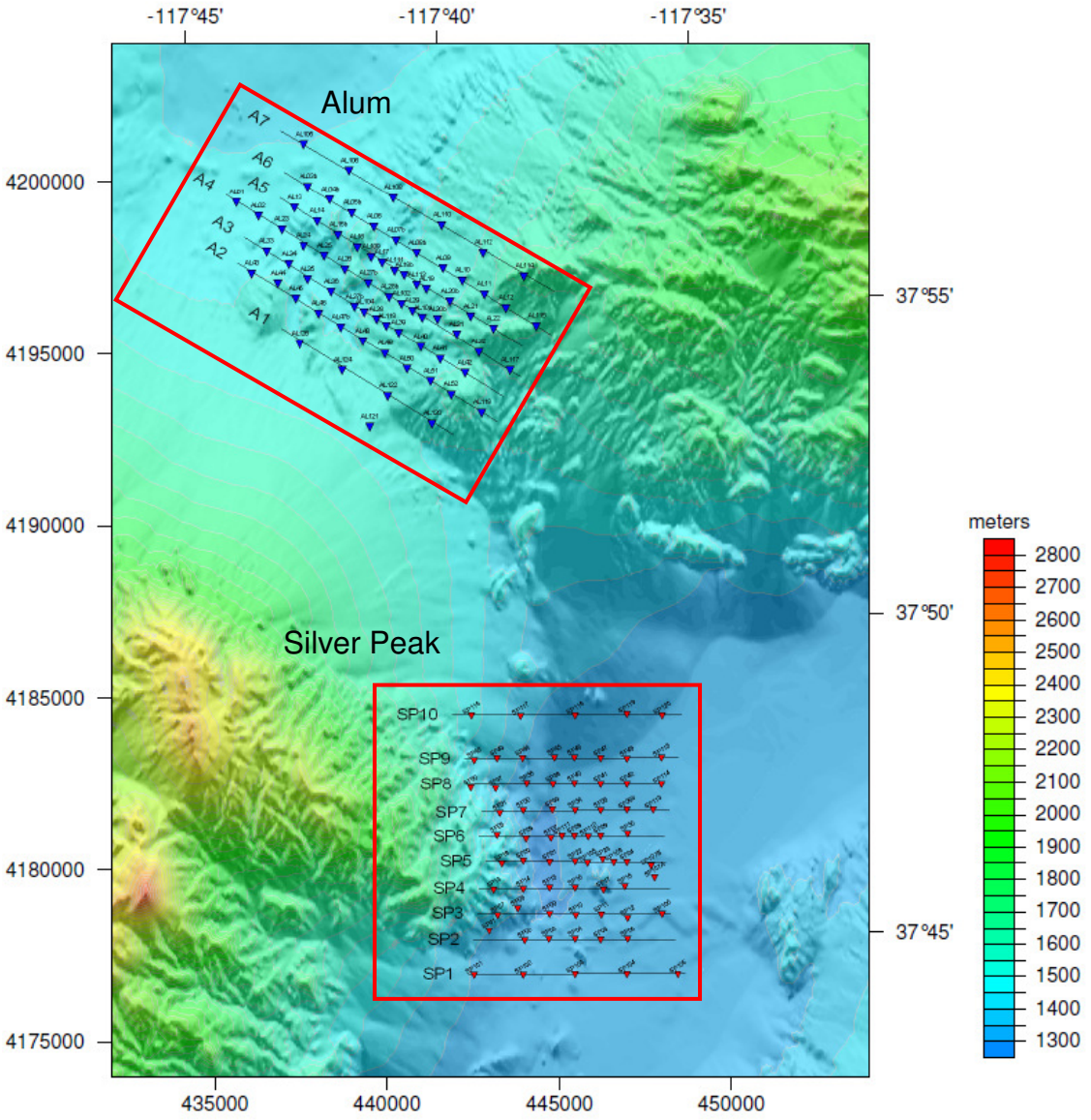

Figure 1. MT station and profile locations on topographic base map (Transverse Mercator, NAD 83).

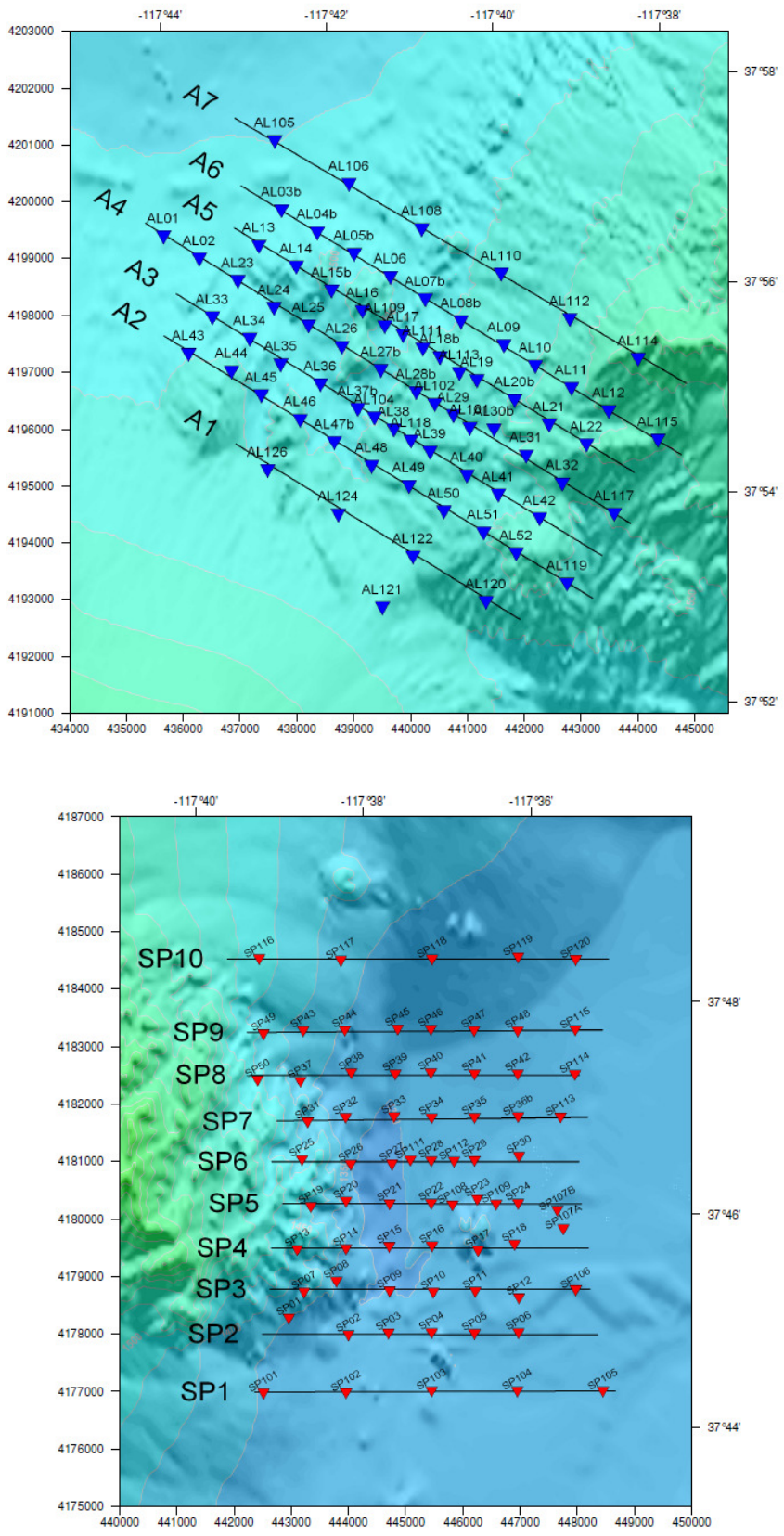

Figure 2. MT station and profile locations on topographic base map for Alum (top) and Silver Peak survey areas (bottom).

All map coordinates are reported in the following system:

Metric Coordinates:	Projection:	Transverse Mercator
	True Origin	117°00' W, 0°00' N
	Coordinates at Origin	500,000m E, 0.000m N
	Datum:	NAD 83
	Spheroid:	Geodetic Reference System 1980
Geographic Coordinates:	Datum:	NAD 83
	Spheroid:	Geodetic Reference System 1980
Elevation	Orthometric:	Extracted from 90m (SRTM) DEM, in meters relative to mean sea level

2 MT DATA REVIEW

2.1 DATA COVERAGE, EDITING AND NOISE CONSIDERATIONS

The MT station spacing was nominally 500m for both prospects (Figure 1, Figure 2; see also Plate 1 for a larger scale). Data covering the seven decades range from 0.001 Hz up to 10,000 Hz were processed at all sites; impedance and tipper parameter plots were presented in the Operational Report (Geosystem, 2010).

A total of 73 MT sites were considered sufficiently good to be included in the final Alum 3D inversion. The chosen subset of the dataset was subject to data editing, and masking of noisy or inconsistent data points to exclude them from further analysis and the 3D inversion. Example soundings are shown in paragraph 2.2.2.

All 69 MT sites recorded a Silver Peak were considered sufficiently good to be included in the final 3D inversion. MT site SP107A was repeated in a different location which was far enough allowing us to include this repeat site in the inversion as an additional MT site. Therefore, the total number of 70 soundings was subject to data editing, masking of noisy data points and 3D inversion. Sample MT soundings are shown in Figure 5 and Figure 6 demonstrating the typical data quality.

All displays of resistivity maps and cross-sections in this report show only the sites included in the 3D inversion.

2.2 DATA ANALYSIS

2.2.1 **Alum**

The MT impedance data (apparent resistivity and phase) shown in Figure 3 exhibit relatively low resistivity (<100 Ωm) for the shallow subsurface, underlain by more resistive formations (>100 Ωm). The majority of the sites show a split between the XY and YX curves for frequencies lower than 1 Hz, hence becoming multi dimensional at increasing depths. The MT sites located in the southern and south-eastern part of the survey area show this split to be occurring at higher frequencies, as visible from example sounding AL22 in Figure 3. This can be explained by the difference in the average shallow subsurface resistivity between southeast and northwest regions.

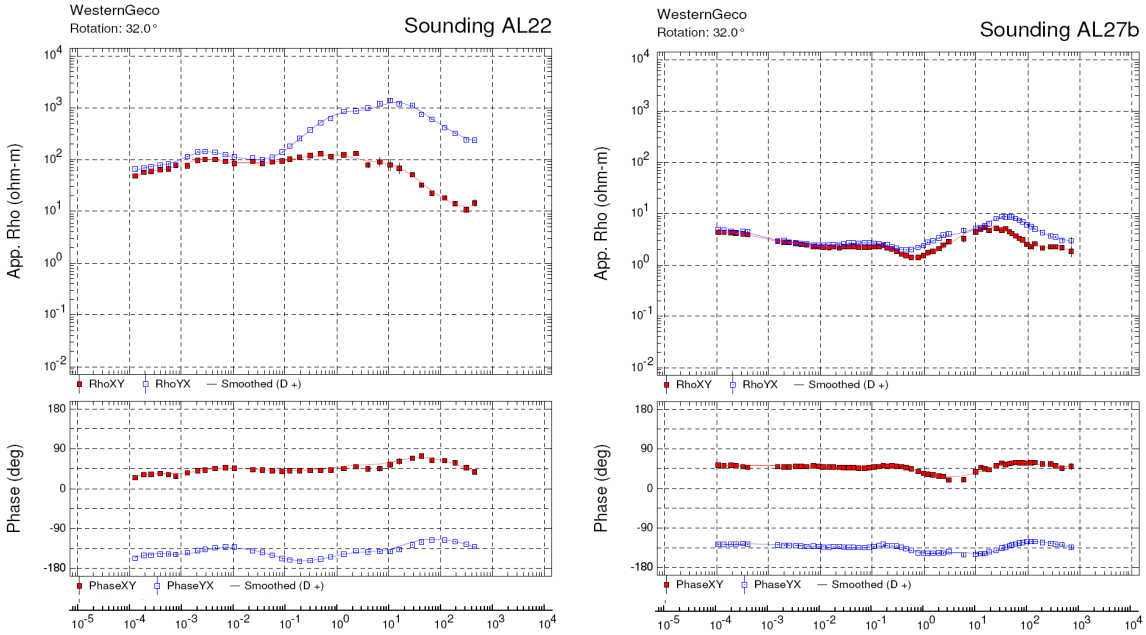

Figure 3. Sample apparent resistivity and phase curves for sites AL22 and AL27b. Data are displayed in N32°E coordinate frame as used in 3D inversions.

Induction vectors, sensitive to lateral resistivity contrasts, are plotted in Figure 4 using the Schmucker convention where the vectors are pointing away from conductors. The vectors are remarkably consistent among the adjacent stations and smoothly change direction and amplitude with frequency. The vectors mainly point away from the low topography particularly at mid frequencies. The amplitude of the induction vectors at high frequencies (300Hz) is small and their directions are scattered, indicating relatively uniform and less resistive features are expected for shallow subsurface. The mid frequency (3-30Hz) Induction vectors are notably different in the southeast and northwest. The magnitude of the vectors in the southeast is larger and consistently pointing towards the high elevations. This may indicate that the relatively uniform conductive feature is deep in the northwest and shallower in the southeast. The large magnitude of the vectors in the southeast also indicates a buried highly resistive zone in this area (Figure 4). Finally, induction arrows at low frequencies (0.03Hz) show a strong regional effect and indicate the most resistive direction to be consistent with the mid periods. However, there is no crossover or significant amplitude reduction occurring towards the northwest which indicates the south-eastern part of the survey area is more resistive at increasing depths as well (Figure 4).

Gridded apparent resistivity and impedance phase invariants are displayed in Figure 5, left and right panels respectively. Apparent resistivity and impedance phase maps show relatively high resistivity (100 Ωm) values near the surface, particularly to the southeast. Two resistive features clearly marked in the induction vector maps are also found in the apparent resistivity maps at 3Hz and 0.3Hz. The diagonal trend shown from induction arrows is well illustrated in the apparent resistivity maps at all frequencies. The correlation of low impedance phase and induction vectors are consistently indicating increasing resistivity in the southeast.

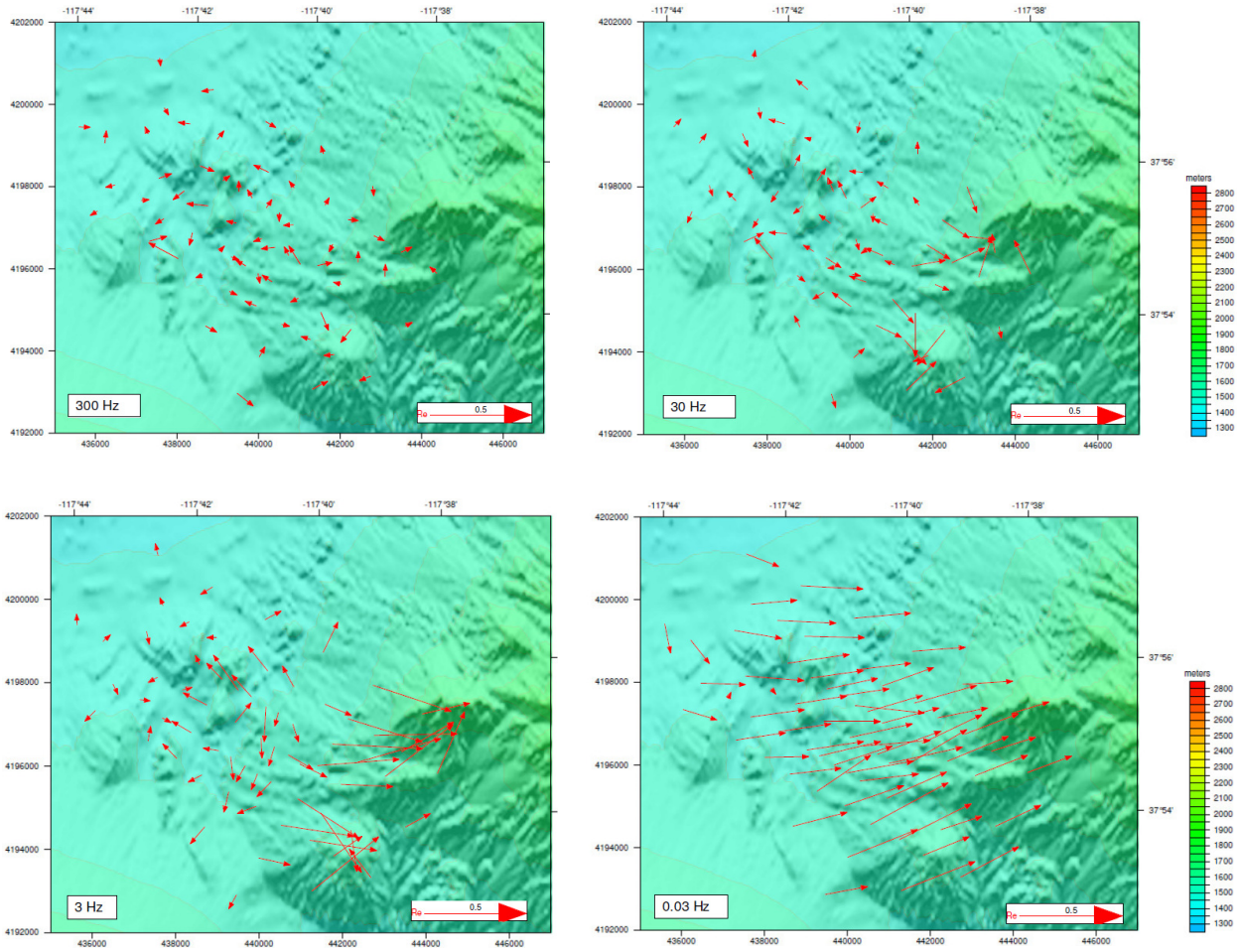

Figure 4. Alum MT data real induction vectors at four different frequencies (300Hz, 30Hz, 3Hz, and 0.03Hz) on shaded topographic relief. In the convention adopted in this report, arrows point away from the conductor.

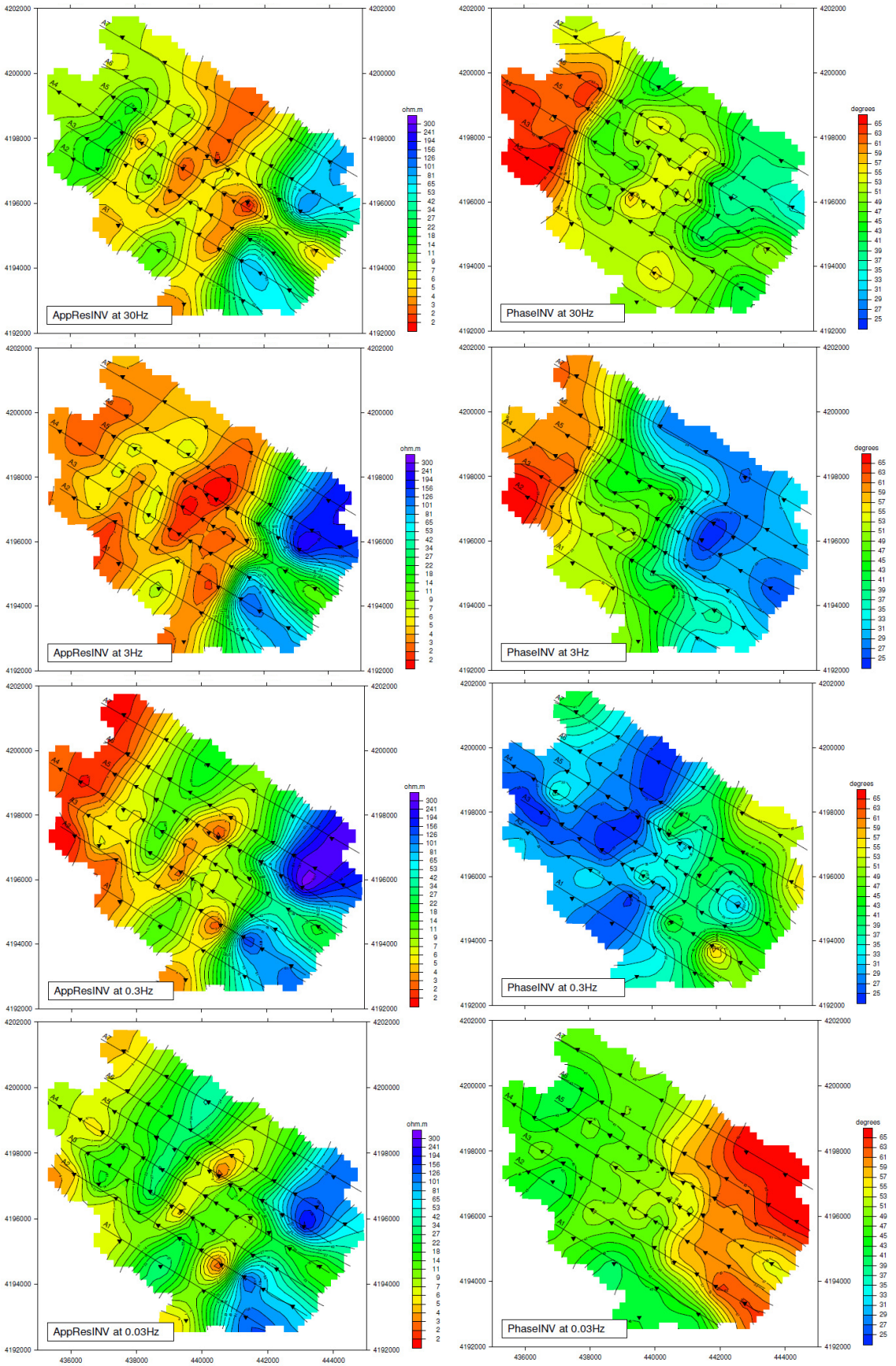

Figure 5. Apparent resistivity invariant (left column) and Phase invariant (right column) for frequencies 30Hz, 3Hz, 0.3Hz, and 0.03Hz.

2.2.2 Silver Peak

The MT impedance data (apparent resistivity and phase) shown in Figure 6 exhibit a structure similar to that observed at the Alum prospect. The split between the XY and YX components occurs around the mid frequencies (~1Hz) implying multi dimensional features are also expected for the Silver Peak area. However, the most conductive and the most resistive areas occur in the eastern and western parts of the survey area respectively. Therefore, the low frequency induction vectors point in opposite directions to the Alum induction vectors at similar frequencies.

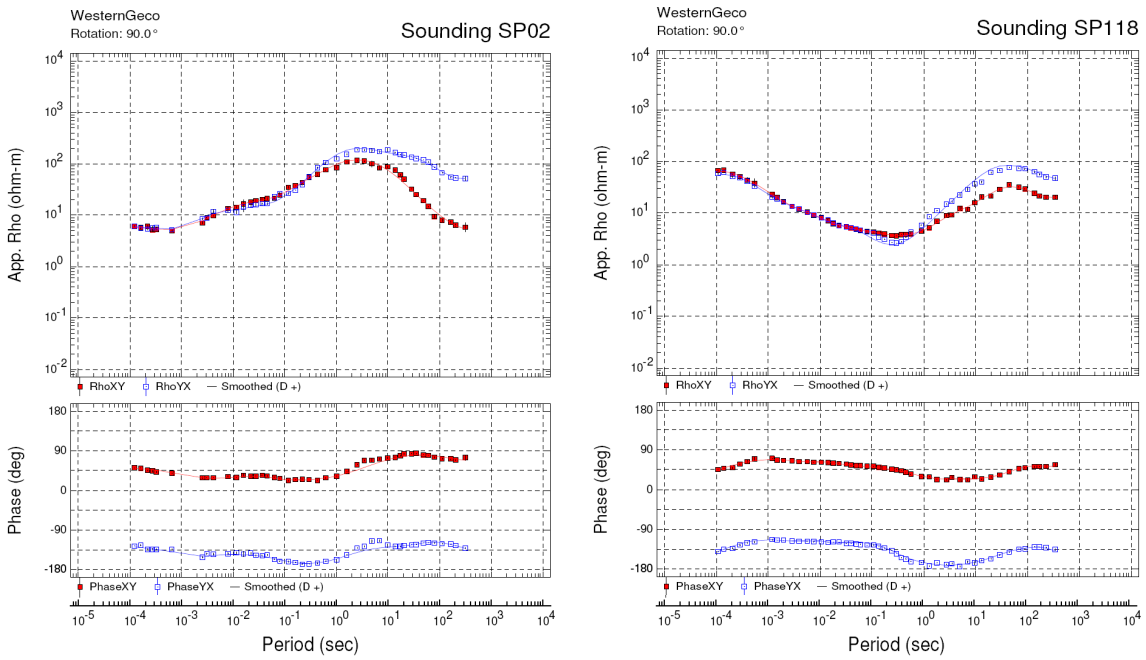

Figure 6. Sample apparent resistivity and phase curves for sites AL22 and AL27b. Data are displayed in N90°E coordinate frame as used in 3D inversions.

Induction vectors for the Silver Peak survey area are shown in Figure 7 using the Schmucker convention where the vectors are pointing away from conductors. Similar to Alum area, the vectors are small and their directions are scattered for high frequency (300Hz) indicating a relatively uniform conductive shallow subsurface. Mid frequency induction vectors in the low elevation part of the area have small amplitudes while the sites on the west, towards the high elevations indicate that this area is more resistive at depth than in the east. Low frequency (0.03Hz) induction vectors have similar magnitudes as those observed at Alum. This indicates the resistivity contrast is expected to be similar at each region. However, the direction of the low frequency induction vectors has reversed, almost pointing in the opposite direction (Figure 7).

Gridded apparent resistivity and impedance phase invariants are displayed in Figure 8, left and right panels respectively. The apparent resistivity and impedance phase maps show low resistivity values for the predominant part of the survey area starting from shallow depths. The apparent resistivity for the high to mid frequencies is almost an order of magnitude lower than the low resistivity part of the Alum area. Lateral resistive-conductive transition on the apparent resistivity maps (Figure 8) is consistent with the increased induction vector amplitudes at 30 Hz and 3 Hz (Figure 7).

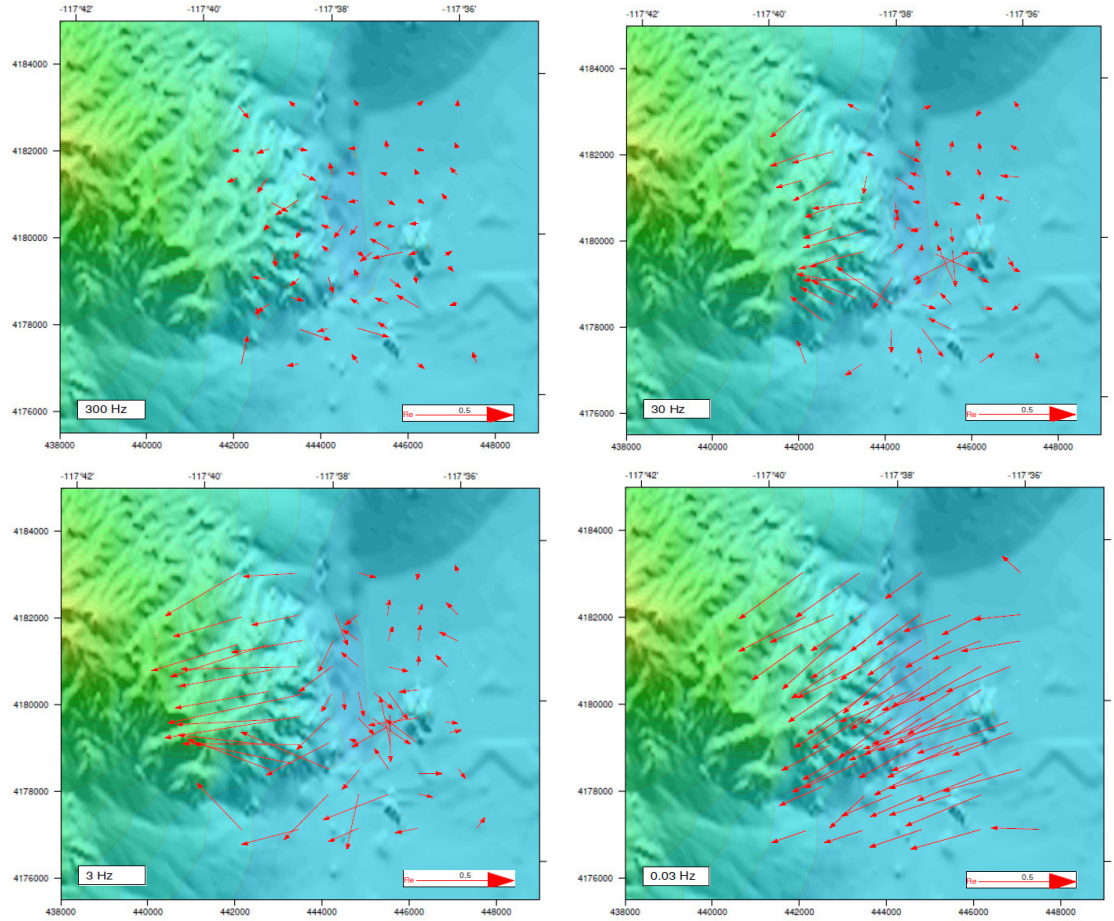

Figure 7. Silver Peak MT data real induction vectors at four frequencies (300Hz, 30Hz, 3Hz, 0.03Hz) on shaded topographic relief. In the convention adopted in this report, arrows point away from the conductor.

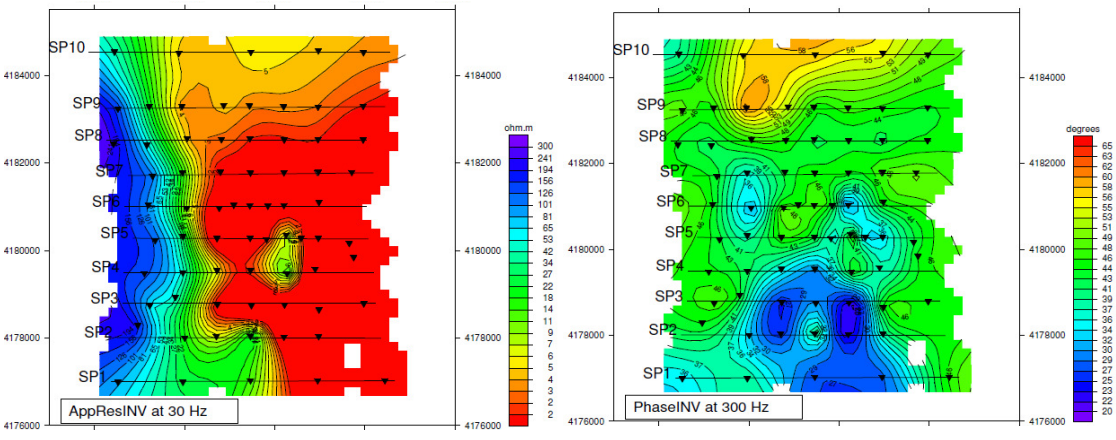

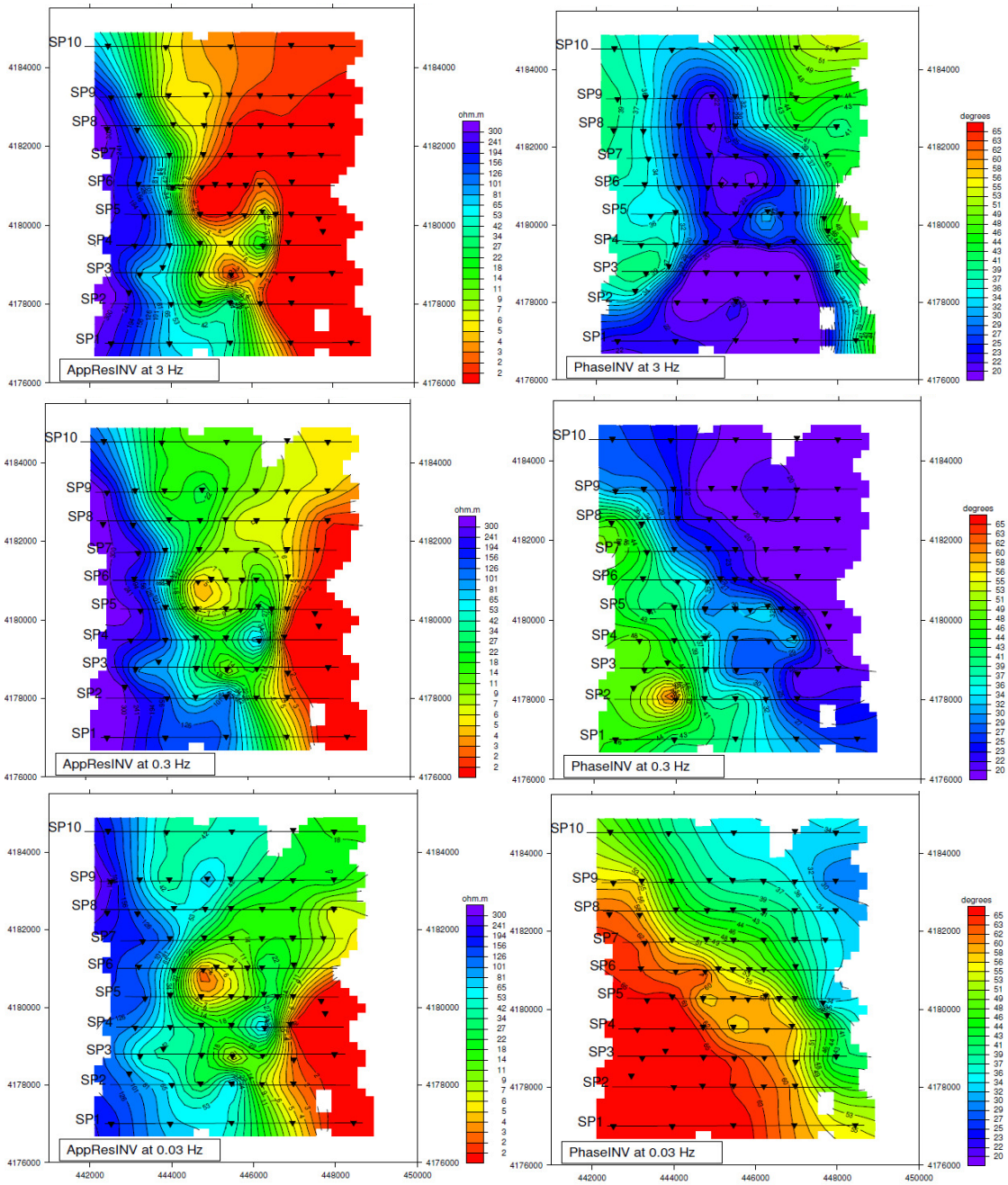

Figure 8. Apparent resistivity invariant (left column) and Phase invariant (right column) for frequencies 30Hz, 3Hz, 0.3Hz, and 0.03Hz.

3 MT MODELING – 3D INVERSION

Numerical electromagnetic modelling was carried out in 3D. Modelling studies used 3D inversion codes described by Mackie and Madden (1993) subsequently implemented and developed by Geosystem from the original routines described in Rodi and Mackie (2001). The regularization operator produces a smoothly varying resistivity volume, consistent with the gradual resistivity changes expected within a geothermal system.

Edited MT data were used for the inversions, checked for outliers due to noise and some data points were masked to avoid single point bias. A summary of the 3D modelling technique is given in Appendix B.

3.1 Mesh dimensions: Alum

The 3D mesh is oriented in E 58°N direction (positive clockwise), and extends considerably beyond the area of interest (horizontally and vertically) in order to avoid model boundary issues (Figure 9). On the other hand the dimensions of the mesh (number of cells) need to be designed in order to achieve a result in reasonable computation times but with sufficient accuracy. The final 3D inversion models used 150x150m spacing for the horizontal directions (X and Y). The vertical mesh thickness was kept 15m throughout the topography. The vertical mesh spacing was gradually increased by a factor of 1.1 until the thickness reached 100m which was increased again after approximately 5km depth. The total model dimension was 89×92 km^2 laterally by 60km depth, with a total of 72×94×122 cells in the X, Y and Z dimensions respectively.

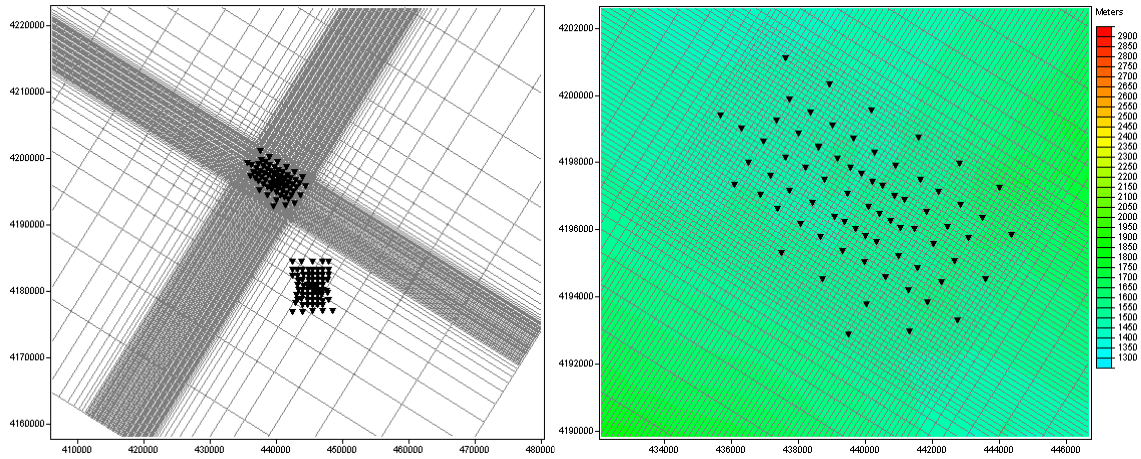

Figure 9. Plan views of full 3D model mesh (Left) and fine mesh centred on Alum MT station locations (Right). Background grid is topography (SRTM DEM – 90m).

3.2 Mesh dimensions: Silver Peak

The 3D mesh is oriented in E 0°N direction (positive clockwise), and extends considerably beyond the area of interest (horizontally and vertically) in order to avoid model boundary issues (Figure 10). On the other hand the dimensions of the mesh (number of cells) need to be designed in order to achieve a result in reasonable computation times but with sufficient accuracy. The final 3D inversion models used

150x150m spacing for the horizontal directions (X and Y). The vertical mesh thickness was kept 10m throughout the topography. The vertical mesh spacing was gradually increased by a factor of 1.05 until the thickness reached 100m which was increased again after approximately 5km depth. Total model dimension was 72×74 km^2 laterally by 53km depth, with a total of 78×88×141 cells in the X, Y and Z dimensions respectively.

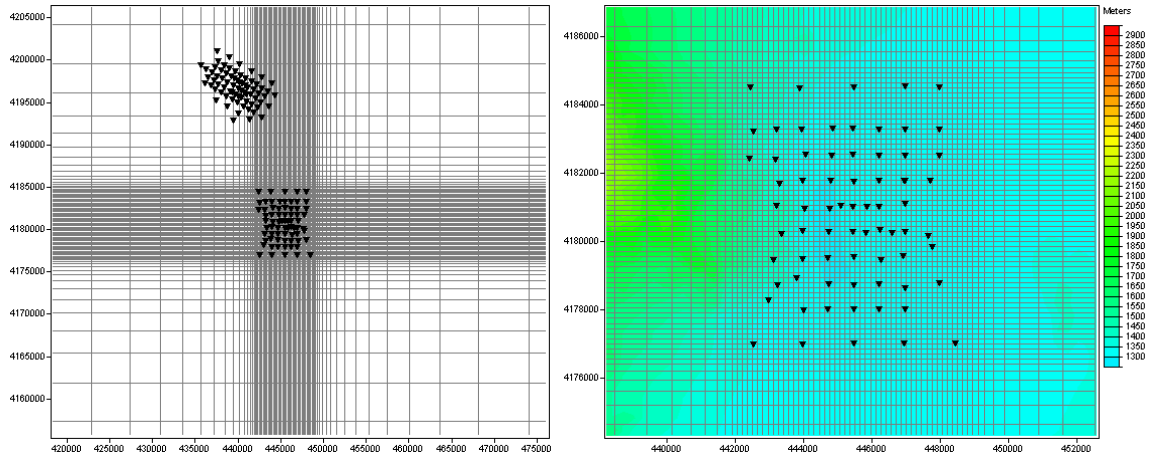

Figure 10. Plan views of full 3D model mesh (Left) and fine mesh centred on Silver Peak MT station locations (Right). Background grid is topography (SRTM DEM – 90m).

3.3 Topography

The 3D mesh and computations included topography from a 90m digital elevation model, extracted from the SRTM (Shuttle Radar Topography Mission). This is an essential practice in this terrain. The model elevations consider an area larger than MT site locations to avoid boundary issues and to take into account terrain variations close to the survey area: elevations of the MT site locations range from roughly 1300m to 1800m msl. In particular elevations range vary from 1800m msl (south of Lone Mountain) to 1450m in Alum survey area, and from 1600m msl (east of Vanderblit Peak) to 1300m in Silver Peak survey area. To avoid computational errors, the mesh was checked for isolated cells above the topography before running the models.

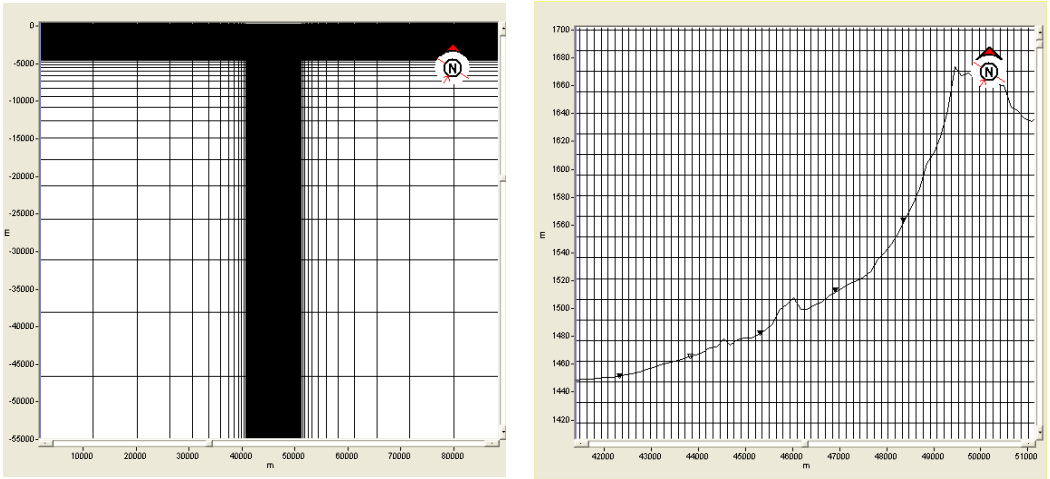

Figure 11. Section views of full 3D model mesh (top) and fine mesh centred on MT station locations (bottom). Background grid is topography (SRTM DEM).

3.4 Inversion parameters

Several 3D inversions were run varying model parameters to achieve a stable result whilst aiming to minimize the RMS misfit (see Appendix C for a detailed list of inversion settings). The data runs successively verified that after editing no soundings were causing "single point" biasing of the 3D model. Following this, model smoothness and regularization were varied, controlled by parameters *tau, alpha,* and *beta* (horizontal *vs*. vertical structure weighting). With lower *tau* the model is freer to satisfy local data misfits and reduce the overall RMS misfit, but at the expense of introducing undue roughness and anomalous, extreme resistivity nodes.

Successive runs were conducted within suites, where the regularization parameter *tau* is lowered between runs to allow for more model structure in later iterations, starting from the previous output (see Appendix C).

For the final set up, parameters were maintained similar to the previous suites; reducing the initial number of frequencies allowing the inversion to quickly reach a smooth model as a starting step for the next lower tau.

The frequency range and number of frequencies used per decade influence the depth range controlled by the model and the model detail respectively. Both final models (#08) ran over the frequency range 0.003 to 1000 Hz, with 4 frequencies per decade (total 23 frequencies). This model converged to a stable solution, with a regularization parameter *tau* of 0.05. Magnetic tipper data was not included in the final inversion. The misfit is defined in terms of the RMS error as following:

$$\text{RMS error} = \sqrt{\frac{1}{npts}\sum\frac{(obs-pred)^2}{\text{var}}},$$

where *obs* and *pred* are the observed and predicted data responses (real and imaginary impedance tensors elements over the frequency range used and the stations employed in the inversion), *npts* is the number of data points, and *var* is the defined variance. Therefore, decreasing the variance (i.e. the error floors) has the effect of increasing the RMS misfit, and vice-versa. For the final inversion, error floors of 3 and 10 per cent were used for lnZxy, lnZyx and Zxx, Zyy, respectively. The RMS misfits for each sounding, together with other model and response files, are provided on CD in Appendix C.

Examples of computed 3D inversion responses versus observed MT data for each area are shown in Figure 12 and Figure 13 for the Alum and Silver Peak survey areas respectively.

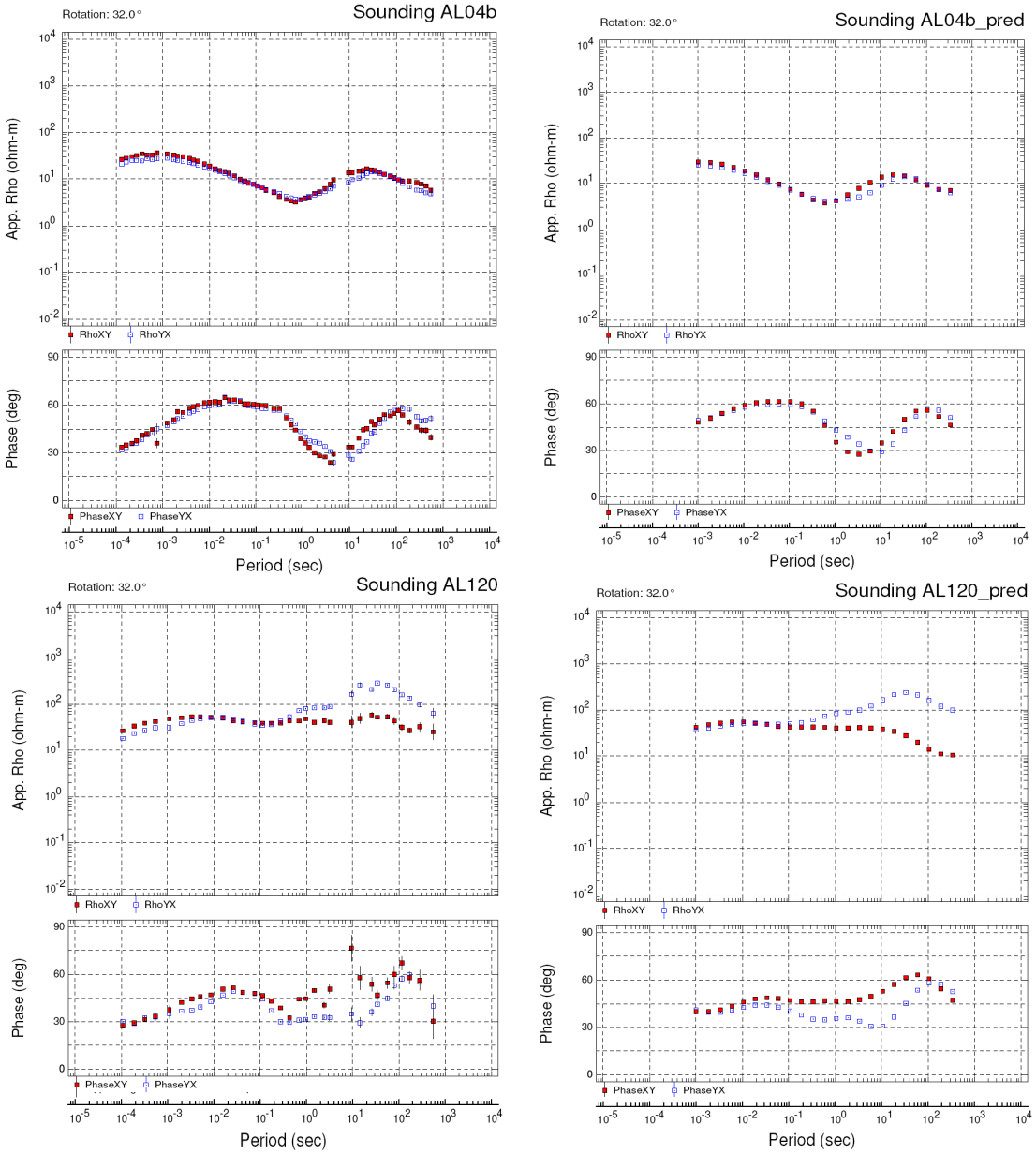

Figure 12. Example MT soundings AL04b (from the north) and AL120 (from the south), showing the fit between observed (Left) and calculated 3D model response (Right). RMS misfit was 1.08 and 2.00 for AL04b and AL120 respectively.

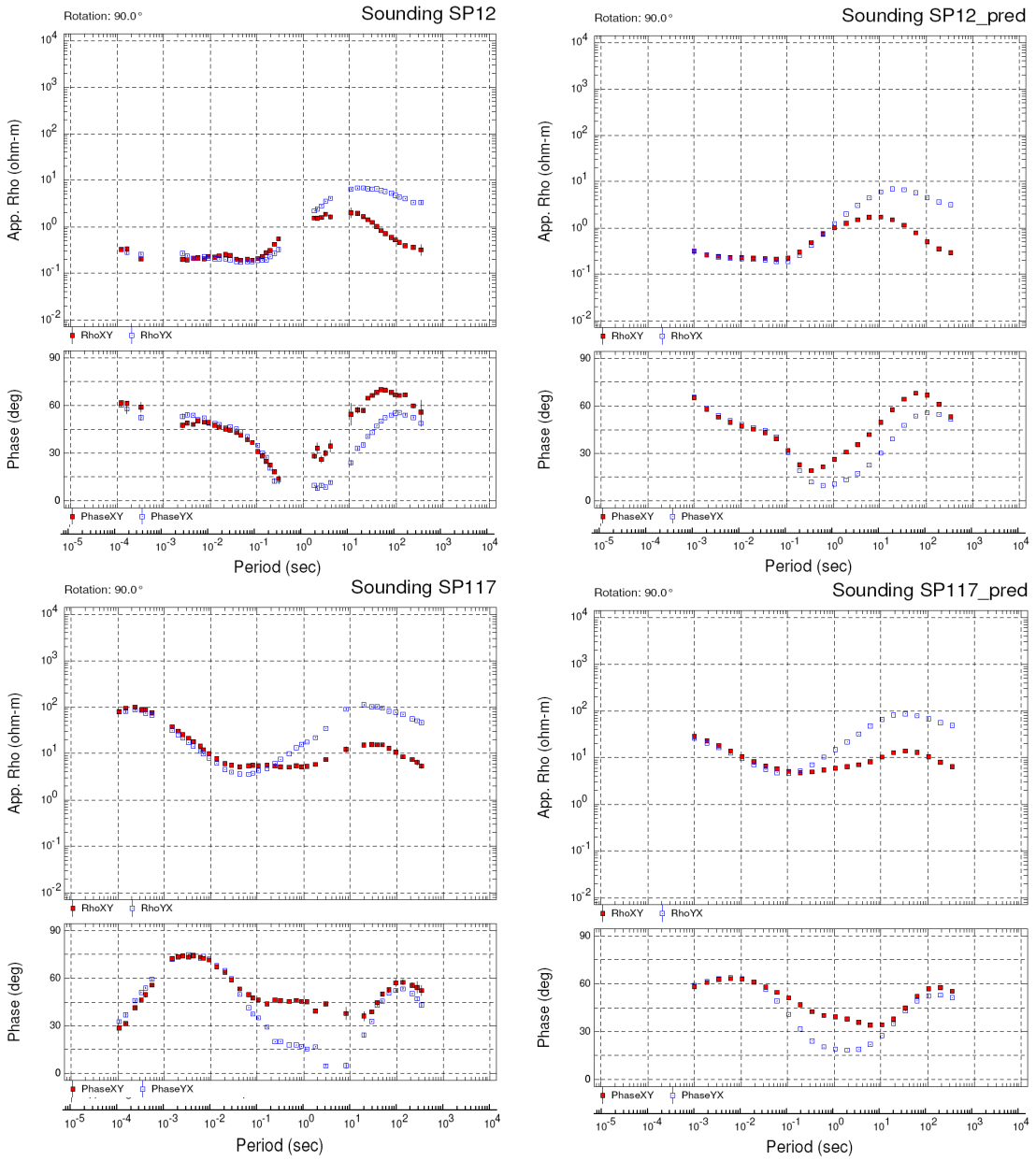

Figure 13. Example MT soundings SP12 (from the southeast) and SP117 (from the northwest), showing the fit between observed (Left) and calculated 3D model response (Right). RMS misfit was 1.50 and 2.51 for SP12 and SP117 respectively.

4 3D INVERSION RESULTS

4.1 Alum

Representative cross-sections and resistivity depth maps are summarized from Figure 14 to Figure 16. Note that these are gridded, interpolated displays of the discrete resistivity mesh cells; the gridding cell size used is 150×60m for the cross-sections, and 150×150 for the maps. Larger scale plots of these are given in the Appendix E.

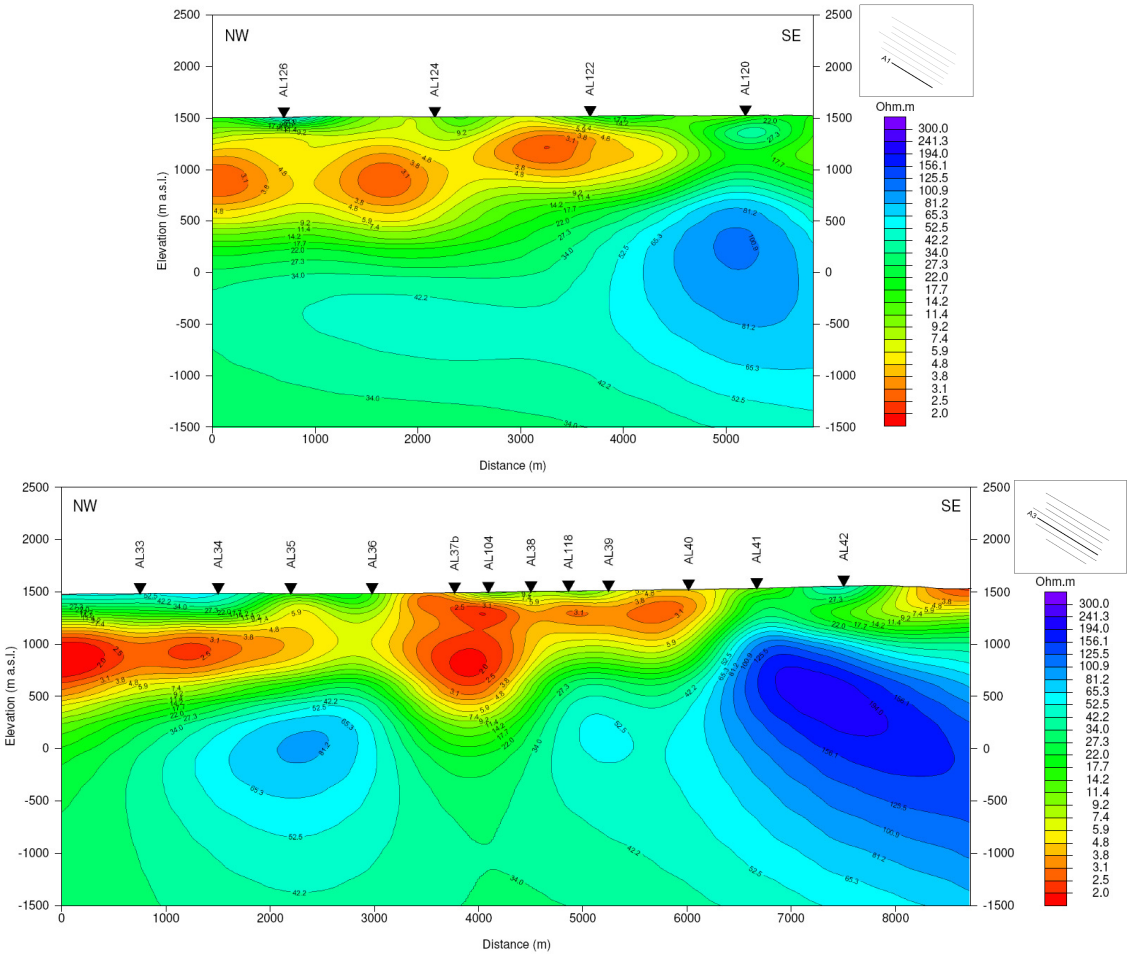

Figure 14. Profiles A1 and A3. Resistivity cross-sections through the final 3D inversion model for Alum survey area. Colour scale is identical in all sections and maps.

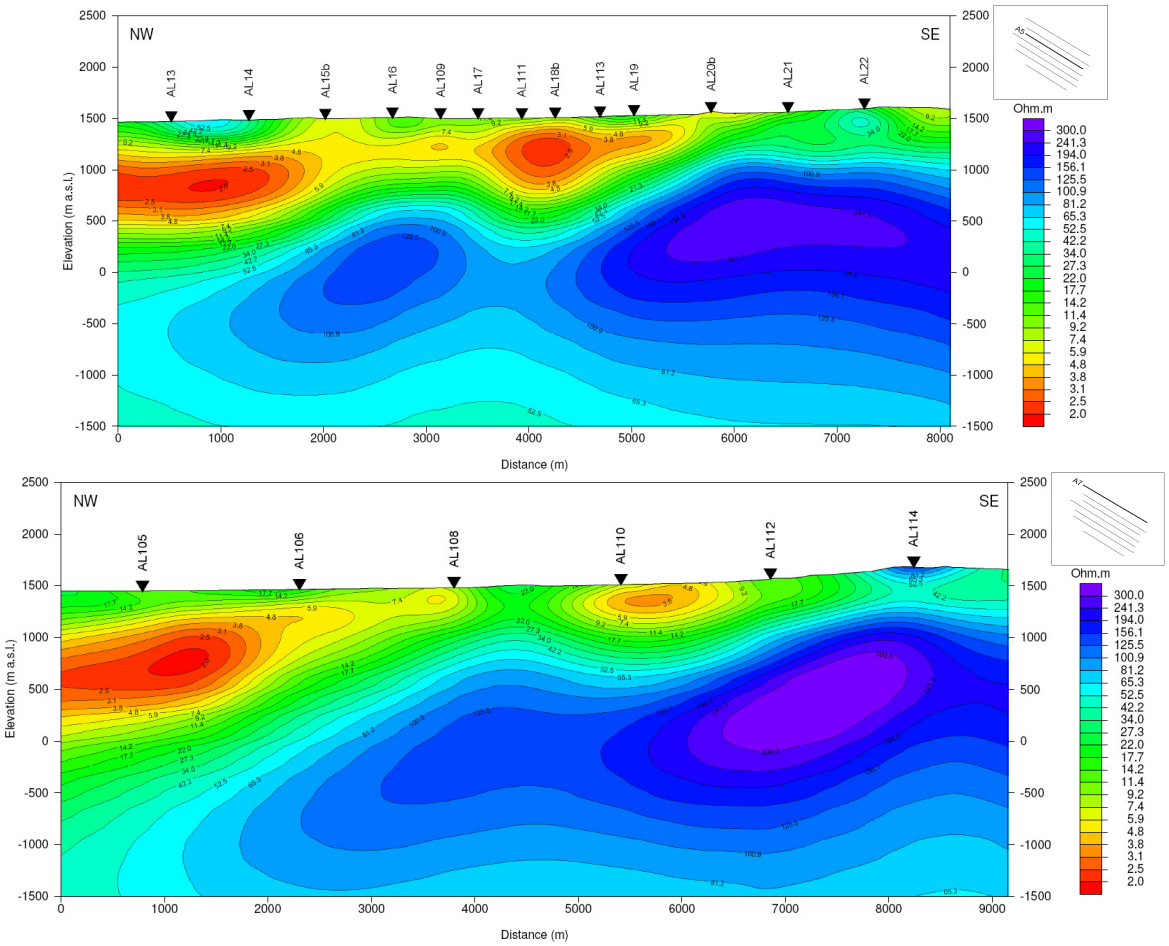

Figure 15. Profiles A5 and A7. Resistivity cross-sections through the final 3D inversion model on Alum survey area. Colour scale is identical in all sections and maps.

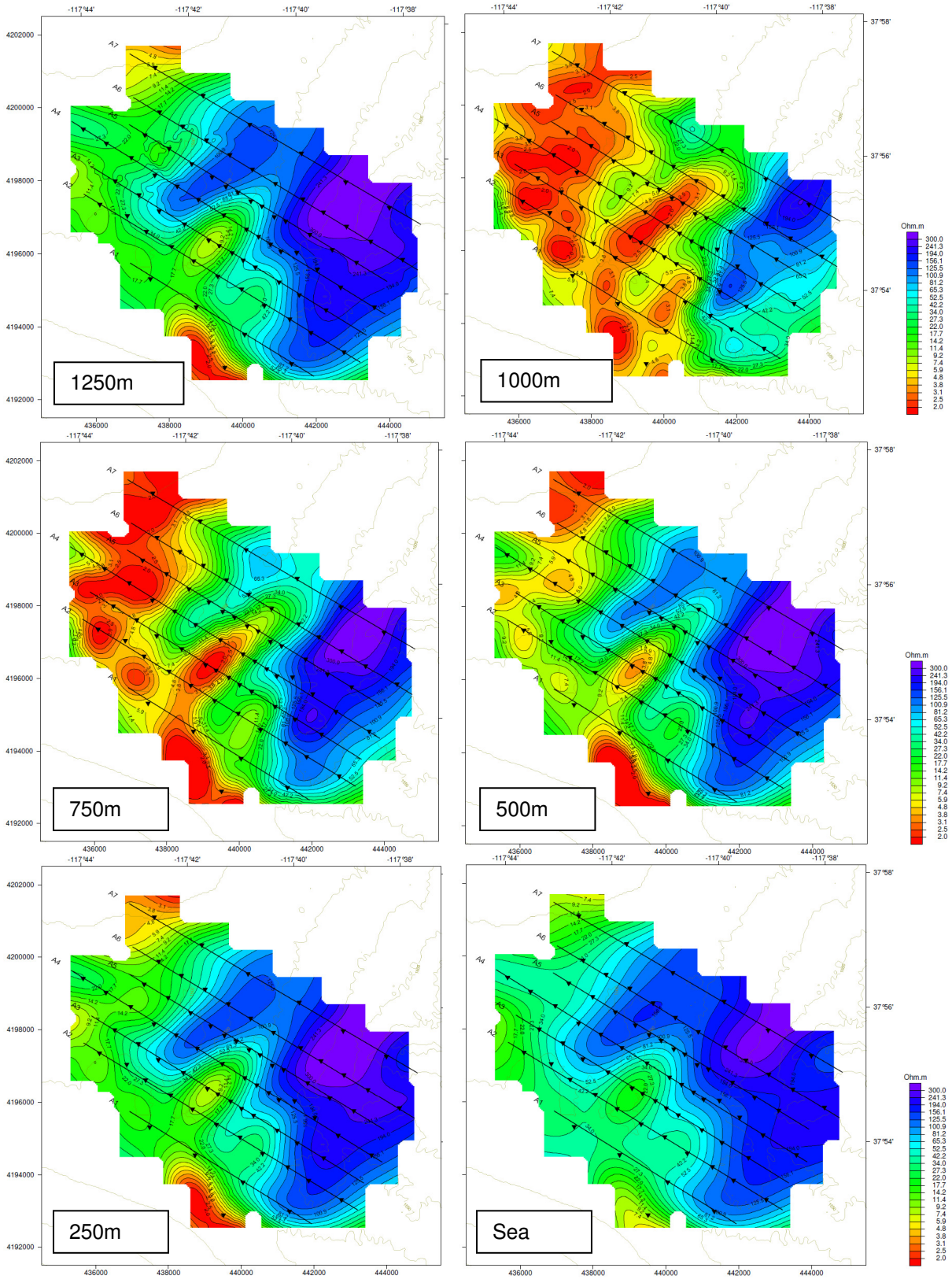

Figure 16. Depth slices through the 3D resistivity model at fixed elevations relative to the mean sea level: 1250m to the Sea level (top left to bottom right).

4.2 Silver Peak

Representative cross-sections and resistivity depth maps are shown from Figure 17 to Figure 19. Note that these are gridded, interpolated displays of the discrete resistivity mesh cells; the gridding cell size used is 150×60m for the cross-sections, and 150×150 for the maps. Larger scale plots of these are given in the Appendix E.

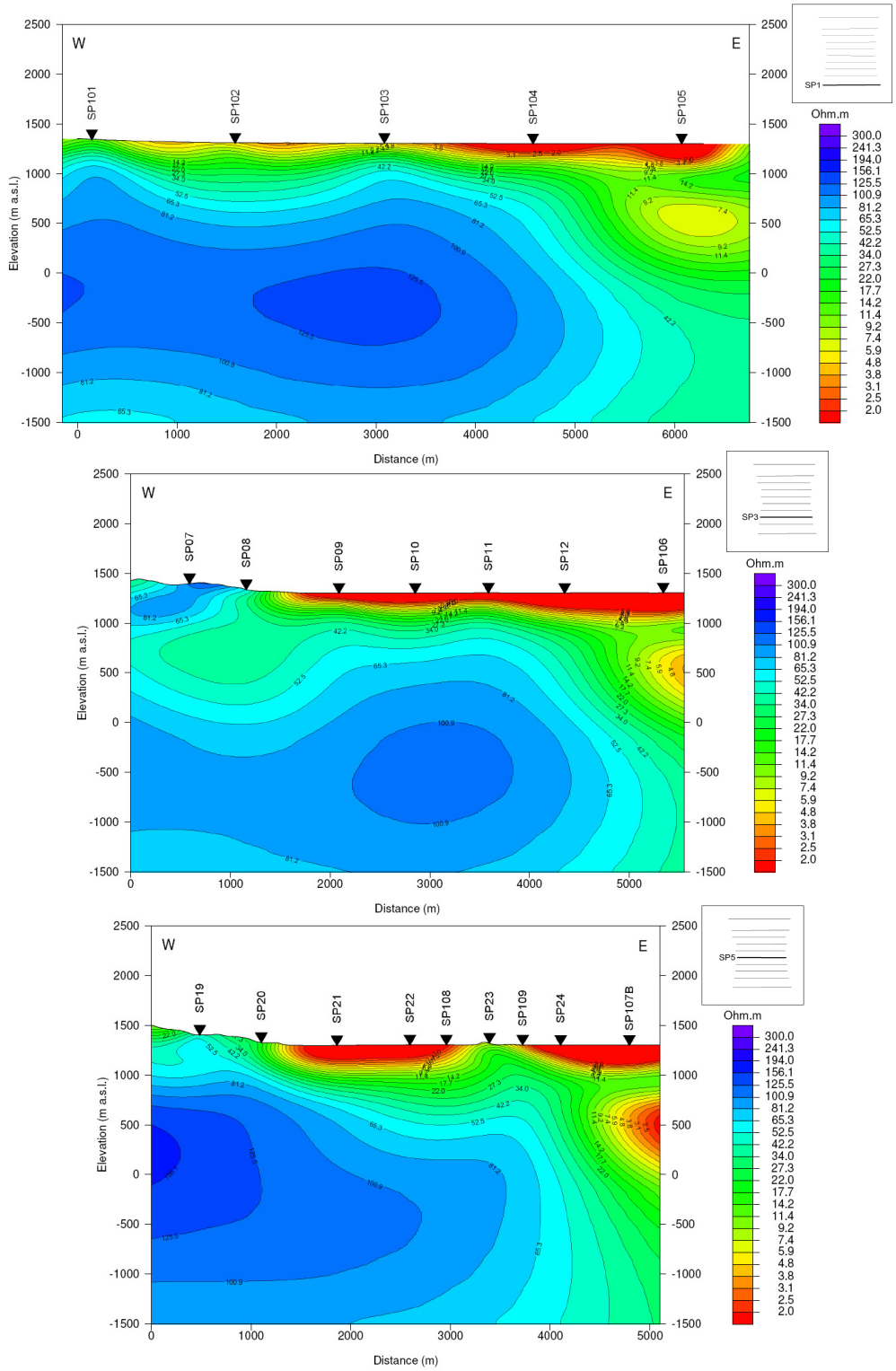

Figure 17. Profiles SP1 SP3 and SP5. Resistivity cross-sections through the final 3D inversion model on Silver Peak survey area. Colour scale is identical in all sections and maps.

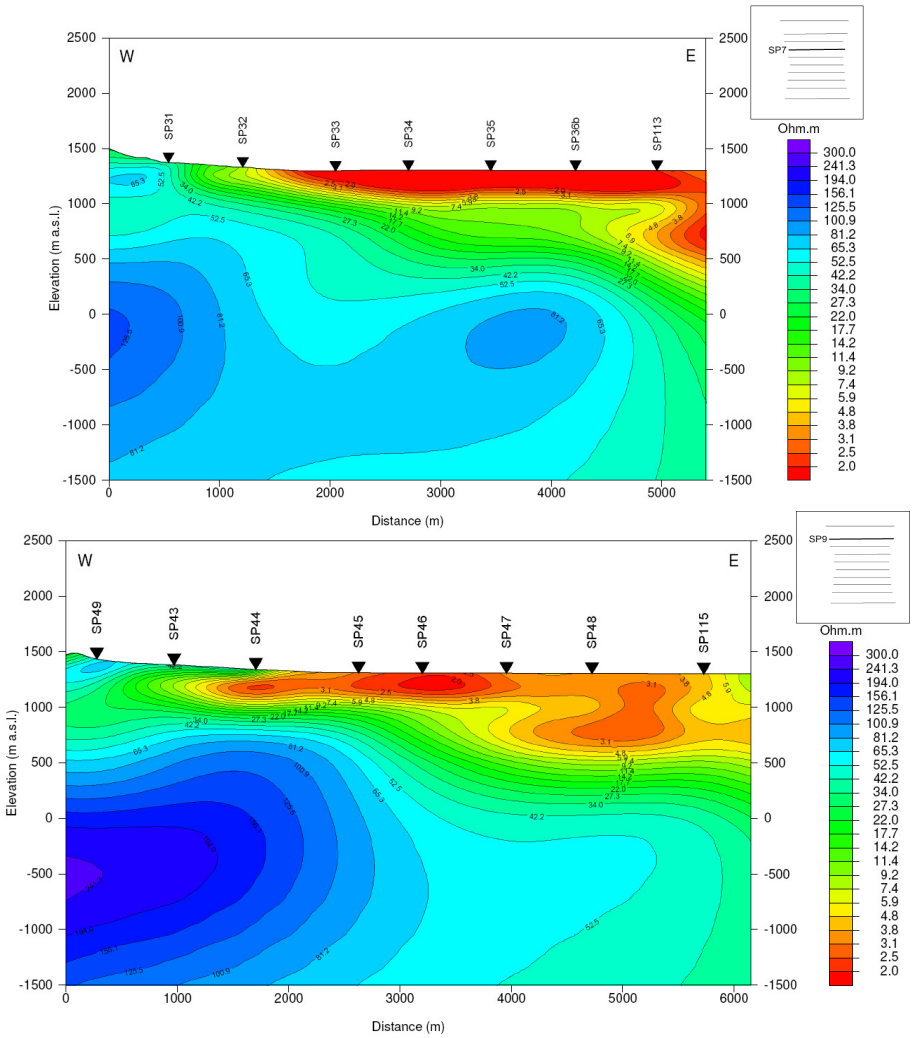

Figure 18. Profiles SP7 and SP9. Resistivity cross-sections through the final 3D inversion model on Silver Peak survey area. Colour scale is identical in all sections and maps.

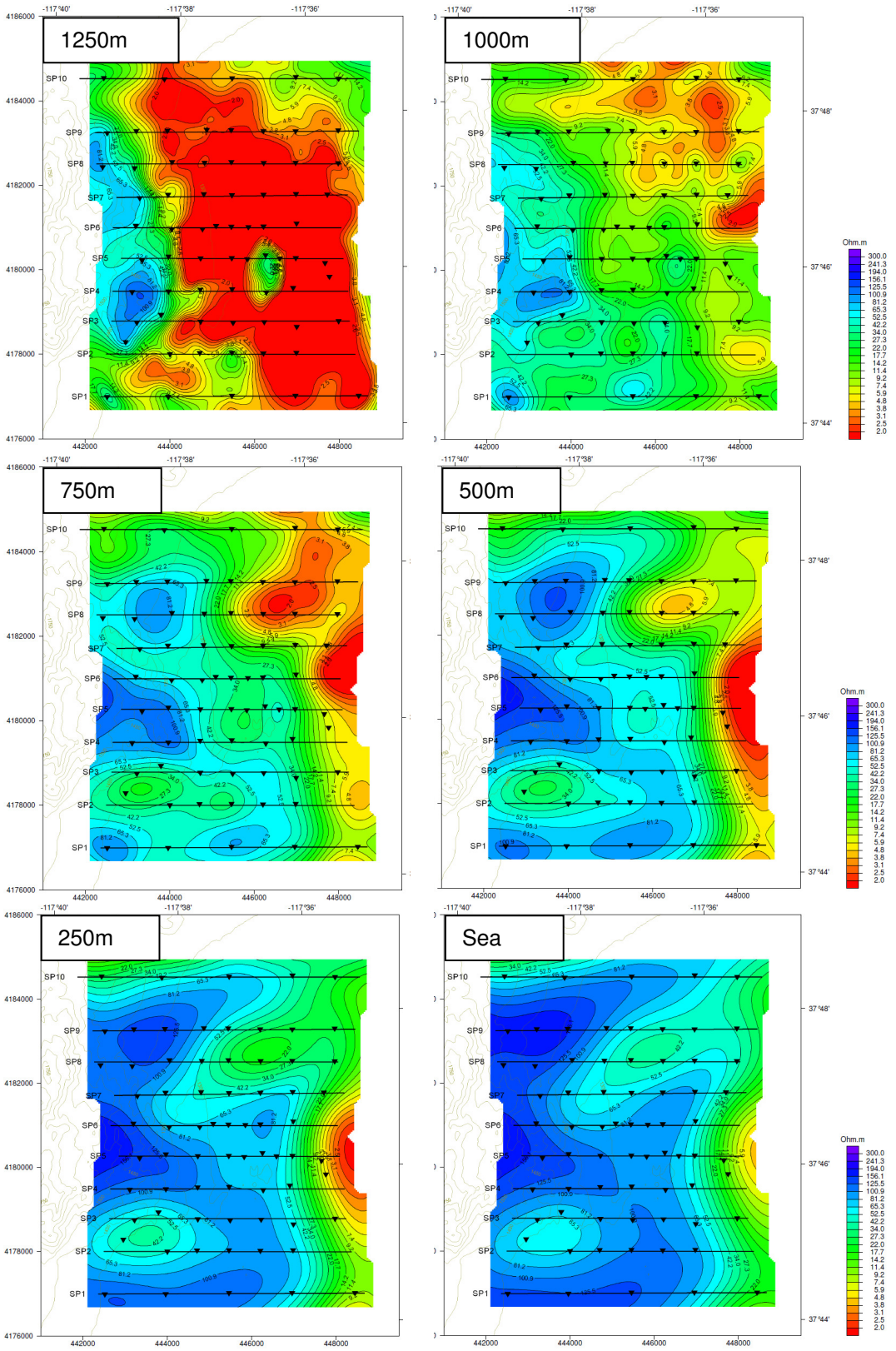

Figure 19. Depth slices through the 3D resistivity model at fixed elevations relative to sea level: 1250m to the Sea level (top left to bottom right).

5 CONCLUSION

Alum and Silver Peak MT data were edited/masked and analyzed for outliers and other inconsistencies before applying the full tensor 3D inversion. The data quality was high in general and majority of the curves had small amount of editing/masking. The edited data were rotated to a coordinate frame to minimize the number of mesh cells and to facilitate 3D inversion computation time.

The final inversion models for both prospects were stable and provided reasonable fit to the observed MT data. Significant resistivity contrasts were imaged laterally and vertically for both survey areas. A low resistivity (1-10 Ωm) surface layer covers highly resistive (>100 Ωm) formations almost throughout the two survey areas. However, the depth to the resistive formation varies gradually within the survey areas. Details of these geoelectrical structures can be seen on the apparent resistivity maps and cross-sections presented in this report as well as larger prints included in the Appendix E.

6 BIBLIOGRAPHY

Andrieux, P. and Wightman, W. E. 1984 The so-called static corrections in magnetotelluric measurements, 54th Ann. Internat. Mtg: Soc. of Expl. Geophys., Session:EM1.1.

Beamish, D., and Travassos, J. 1992 The use of D+ in Magnetotelluric interpretation: J. Appl. Geophys. 29, 1-19.

deGroot-Hedlin, C., and Constable, S. 1990 Occam's inversion to generate smooth, two-dimensional models from magnetotelluric data, Geophysics, 55, 1613-1624.

Fletcher, R. and Reeves, C.M. 1959 Function minimization by conjugate gradients, Computer J., 7, 149-154.

Geosystem 2009 Magnetotelluric Surveys, Alum & Silver Peak, Nevada - USA: Operational report prepared for Sierra Geothermal Power.

Mackie, R.L., and Madden, T.R. 1993 Three-dimensional magnetotelluric inversion using conjugate gradients: Geophys. J. Int., 115, 215-229

Mackie, R.L., Rodi, W., and Watts, M.D. 2001 3-D magnetotelluric inversion for resource exploration: paper PF3.3, Extended Abstracts, Ann. Mtg. SEG

Polak, E. 1971 Computational Methods in Optimization: A Unified Approach, Academic Press, New York.

Press, W.H., Teukolsky, S.A., Vetterling, W.T., and Flannery, B.P. 1992 Numerical Recipes in FORTRAN: The Art of Scientific Computing, Second Edition, Cambridge University Press.

Rodi, W., and Mackie, R.L. 2001 Nonlinear conjugate gradients algorithm for 2-D magnetotelluric inversion, Geophysics, 66, 174-187.

Smith, J.T., and Booker, J.R. 1991 Rapid inversion of two- and three-dimensional magnetotelluric data, J. Geophys. Res., 96, 3905-3922.

Tikhonov, A.N., and Arsenin, V. Y. 1977 Solutions of Ill-Posed Problems, V.H. and Sons: Washington, D.C.

Vozoff, K. 1991 The magnetotelluric method in Electromagnetic Methods in Applied Geophysics, Vol2B 641-711, pub. SEG.

Wannamaker, P.E., Hohmann, G.W., and Ward, S.H. 1984 Magnetotelluric responses of three-dimensional bodies in layered earths, Geophysics, 49, p. 1517-1533.

Zhdanov, M.S. 2002 Geophysical inverse theory and regularization problems: Elsevier, Methods in Geophysics 36.

APPENDIX A GLOSSARY

1D	The earth is assumed to be made up of homogeneous horizontal layers
2D	Geology is assumed to be uniform along strike, but varies in the dip direction.
3D	Geology varies in all 3 directions (x, y, and z)
bgl	Below ground level
bsl (asl)	Below sea level (above sea level)
Coils	Sensors used to measure time-varying magnetic fields
Conductance	For a layer, product of layer thickness × conductivity (Siemens, S). See also Total Conductance, below.
Conductivity	1/resistivity (in S/m).
Contact resistance	Resistance of the electrode pot relative to a ground, measured in Ω.
E-line	Cable used to measure the electric field
EM	Electromagnetic
E_x and E_y	Electric field strengths, in units of mV/km, measured in the x and y directions respectively.
f	frequency, in Hertz (Hz)
H_x , H_y , and H_z	Magnetic field strengths, in units of nT, measured in the x, y, and z directions (z positive upwards).
Induction arrow	Real part of the vector $\lfloor T_x \quad T_y \rfloor$, illustrating the relation between the vertical and horizontal magnetic field components from $H_z = T_x H_x + T_y H_y$, plotted to show direction towards an assumed 2D line-source (i.e. towards the conductor in the so-called reversed convention).
LaToracca skew angle	=90°-(θ_{EH}), where θ_{EH} is the angle between the major axes of the E and H polarization ellipses. Since this angle, should be 90°, the La Toracca skew angle should be zero under 1 or 2 D conditions. In 3D conditions, the E field may be distorted (i.e. rotated), resulting in non-zero values.
m msl	meters above Mean Sea Level
Mode (TE or TM)	In a 2D world, the AMT/MT impedance is decomposed into two orthogonal components parallel (TE, or Transverse Electric) and perpendicular (TM, or Transverse Magnetic) to strike. In 1D and 3D situations the definition has limited value.
Occam inversion	Inverse modeling of geophysical data in which no *a priori* assumptions (e.g. the resistivity/thickness distribution) are made. Rather, the simplest model consistent with the data is found. Named for the 14th century philosopher William of Occam (see Occam, 1324, *Quodlibeta*, Book V: "Plurality is not to be assumed without necessity").
Period	Inverse of frequency (1/f). Commonly used instead of frequency in describing the low frequency range in AMT/MT (defined in seconds, s)
Pot	Potential electrode: sensor at the end of the E line for measuring the electric field

ρ	apparent resistivity in Ωm
ρ_{max} and ϕ_{max}	The higher of the two apparent resistivity curves and its associated impedance phase.
ρ_{xy}	apparent resistivity calculated from E_x and H_y
ρ_{yx}	apparent resistivity calculated from E_y and H_x
RMS error	$\sqrt{\frac{1}{npts}\sum\frac{(obs-pred)^2}{\text{var}}}$ where *obs* and *pred* are the observed and predicted data responses (real and imaginary impedance tensors elements over the frequency range used and the stations employed in the inversion), *npts* is the number of data points, and *var* is the defined variance.
Roughness (of 3D resistivity model)	This is defined as the integral over the 3D model of $L^TL \cdot m$, where L is the Laplacian and m is the model resistivity. Interfaces in the resistivity are indicated in the model volume by zero-crossings in Roughness. In that this parameter is a fourth derivative, it is inevitably prone to noise, but in compensation aids in identifying the most likely position of an interface.
Sensitivity Matrix, A^TA	The sensitivity matrix $A^T A \equiv \frac{\Delta(response)}{\Delta(model)}$ represents the amount of change in the modeled data due to a small change in the model parameter. This shows the sensitivity of the response to a particular 3D model, for each cell of this 3D mesh.
Static shift	Frequency-independent shift of AMT/MT apparent resistivities along the resistivity axis, caused by local electric field distortion.
Static stripping	A method of correcting static shift. At a user-selected (normally high) frequency the impedance is forced to a uniform 1D solution at the actual rotation angle, such that xy and yx apparent resistivities have identical absolute values. The corresponding e-field correction is then applied for all frequencies, and impedance re-calculated at the same orientation angle. Stripping therefore attempts to correct static shift via the impedance distortion, rather than simply block-shifting the (derived) apparent resistivity curves.
TD	Total depth (of a well).
Tipper	Ratio of the vertical magnetic component H_z to the horizontal magnetic field components H_x and H_y. Since the vertical component (noise excluded) is the output of a system (the earth) to which the two horizontal components are the input, its absolute value should not exceed 1 (see *induction arrow*).
Tipper strike	The geographic orientation in the horizontal plane of the vector relationship between the magnetic field components (*tipper*), taking real and imaginary parts into account. In a *2D* earth, the tipper strike is perpendicular to the induction arrow direction, and shows the um *2D* geo-electric strike.

Top of conductor	A surface interpreted from a resistivity distribution (e.g. 1D layered earth models or 3D resistivity volume in the MT case) depicting the elevation of the top of the (principal) conductive horizon. Shown as contour map or line on cross-section. Units are m msl.
Total conductance	The conductivity (=1/resistivity), integrated to a specified depth z: TC= $\sum_{0}^{z} \Delta z_i / \rho_i$, where Δz is the thickness of the *i*th layer and ρ_i its resistivity.

APPENDIX B 3D MT INVERSION

B.1 AN INTRODUCTION TO 3D MT INVERSION

The general approach to the inversion of geophysical data consists of two steps: (1) the computation of a forward response, and (2) the comparison of this with observed data, and modification of the starting model in light of the differences between observed and computed data. To be reasonably practical, this requires a fast forward code and an efficient approach to inversion.

B.2 3D FORWARD MODELING

3-D MT data are derived from measurements at Earth's surface of naturally occurring electric and magnetic fields. A standard 3-D MT dataset usually comprises four complex quantities (impedances) as a function of receiver position and frequency. The four impedances observed in 3-D MT, then, are the components of a 2 x 2 impedance tensor. Modeling of the impedance tensor entails solving Maxwell's equations in the solid earth and atmosphere using a horizontal current source in the atmosphere to represent ionospheric and magnetospheric sources. In our modeling algorithm we divide the earth and atmosphere into rectangular blocks with the magnetic fields defined along the block edges and the electric fields defined along the normals to the block faces (Mackie et al., 1994). Finite difference equations can be easily derived using this formulation. If one eliminates the electric fields from the difference equations, one obtains a second-order set of equations in H. This system of equations is sparse, symmetric, and complex (all elements are real except for the diagonal elements). The solution to this system is obtained by use of the stabilized biconjugate gradient algorithm. Convergence is speeded up by use of a preconditioner that is the incomplete Cholesky decomposition of the diagonal sub-blocks with fill-in plus a correction for the divergence of the magnetic field (Mackie et al., 1994). Once the E and H fields have been determined for two linearly-independent source polarizations, the impedance tensor can be computed.

B.3 3D INVERSION

The general magnetotelluric inverse problem is posed in canonical form and solved using the framework of Tikhonov regularization (Tikhonov and Arsenin, 1977). Following many previous workers in MT inversion, a smooth, or `minimum-structure', resistivity model that gives acceptable fits to the observed data is sought. Thus, using a simple second-order operator, solutions are models with minimum spatial variability, or roughness. The method of nonlinear conjugate gradients (NLCG) is used to minimize the misfit; nonlinear conjugate gradients are a well-known optimization method (Fletcher and Reeves, 1959) which has been applied in a variety of nonlinear geophysical inverse problems, e.g., Ellis and Oldenburg (1994). While NLCG is a general method for optimization, it is not necessarily efficient in a computationally intensive problem like 2-D and 3-D MT inversion. The efficiency of NLCG for computing solutions of the inverse problem depends strongly on the preconditioner and the line minimization algorithm. The purpose of these is to steer the gradient into a direction in model space which parallels the final solution as much as possible. A restriction on this goal is that applying the preconditioner can require an excessive amount of computation if it is too complicated. It is applied to a

parameter vector by solving the linear system, which can therefore be applied efficiently, acting in some sense like the inverse Hessian matrix. The amount of computation needed to solve the system is less than one forward function evaluation and thus adds little overhead to the algorithm. Line minimization is only a one-dimensional problem, requiring the computation of at least one forward problem, which in 3-D MT is computationally demanding. It is thus very important to use an algorithm that does a reasonable job in the current search direction with as few trials as possible. Algorithms such as that in Press et al. (1992) do not achieve this goal. In our 3-D MT algorithm, we use a line minimization algorithm that is basically a univariate version of the Gauss-Newton method. While details of this algorithm are given in Rodi and Mackie (2001), the important result of this algorithm is that each step of the line minimization iteration requires the equivalent work of only three MT forward calculations (the real one and two pseudo ones). An additional efficiency is our choice of stopping criterion. It ensures that, when the forward problem is well-approximated by its linear approximation, each line minimization converges in a single step.

The net result is that the observed 3D data (each element of the impedance tensor, at each frequency used) can be inverted to give a smooth 3D model. The method is efficient and fairly fast: for example, the Alum model with 825,696 cells, 73 sites, and 23 frequencies – for 74 cumulative iterations took approximately 100 hours of CPU time (parallel cluster with 120 nodes running the Linux operating system).

Smooth model inversions are quite useful for geologic interpretations because they provide accurate representations of the subsurface. Their disadvantage, however, is that they do not resolve sharp boundaries or interfaces. Rather, because of the smoothness constraint, interfaces are defined in general terms by resistivity gradients. Practically, however, what is of interest is the depth to a particular interface or geologic formation. In those situations where additional information is available (e.g., well logs, seismic, etc), we can use that information to generate a “tear surface” which we then project onto the MT model. Across this surface, we turn off the smoothing constraint and allow the resistivities to vary independently above and below the surface. If the geology is well approximated by this surface, then the resulting model will in general be smooth except across this surface. In this way, we can introduce sharp boundaries into the 3D MT inversion.

APPENDIX C PRINCIPAL 3D MODEL PARAMETERS

C.1 ALUM SURVEY AREA

Setup	iterations	cumulative its	rms	start model	tau	tipper inversion	lnZxy/yx error floor	Zxx/yy error floor	tipper error floor	tau (m-m0)	min resistivity	max resistivity	static shift	orientation [deg]	nx	ny	nz	min dx, dy [m]	min dz [m]	deep dz [m]	# sites	# frequencies	# freqs / decade	min frequency	max frequency	Version code
01_Nov20	56	56	1.906	20	3	n	3%	10%	-	0.03	0.2	50000	n	58	54	89	129	150	20	100	52	24	4	0.003	1000	1.1.6
02_Dec29	20	20	2.148	20	10	n	3%	10%	-	0.03	0.1	10000	n	58	68	90	122	150	15	150	73	23	4	0.003	1000	1.1.6
03_Dec30	30	30	1.842	02_20iter	3	n	3%	10%	-	0.03	0.1	10000	n	58	68	90	122	150	15	150	73	23	4	0.003	1000	1.1.6
04_Jan27	20	20	2.256	20	10	n	3%	10%	-	0.03	0.1	10000	n	58	72	94	122	150	15	100	73	23	4	0.003	1000	1.1.6
05_Jan29	20	40	1.914	04_20iter	3	n	3%	10%	-	0.03	0.1	10000	n	58	72	94	122	150	15	100	73	23	4	0.003	1000	1.1.6
06_Jan31	30	70	1.688	05_20iter	1	n	3%	10%	-	0.03	0.1	10000	n	58	72	94	122	150	15	100	73	23	4	0.003	1000	1.1.6
04_randy_test	23	23	2.357	20	0.1	n	3%	10%	-	0.03	0.1	10000	n	58	72	94	122	150	15	100	73	6	1	0.003	300	1.1.6_3
07_Feb26	39	62	1.686	04r_23iter	0.05	n	3%	10%	-	0.03	0.1	10000	n	58	72	94	122	150	15	100	73	23	4	0.003	1000	1.1.6_3
08_Mar01	**12**	**74**	**1.589**	**07_39iter**	**0.01**	**n**	**3%**	**10%**	**-**	**0.03**	**0.1**	**10000**	**n**	**58**	**72**	**94**	**122**	**150**	**15**	**100**	**73**	**23**	**4**	**0.003**	**1000**	**1.1.6_3**

The final model presented in this model is #08 in the list.

C.2 SILVER PEAK SURVEY AREA

Setup	iterations	cumulative its	rms	start model	tau	tipper inversion	lnZxy/yx error floor	Zxx/yy error floor	tipper error floor	tau (m-m0)	min resistivity	max resistivity	static shift	orientation [deg]	nx	ny	nz	min dx, dy [m]	min dz [m]	deep dz [m]	# sites	# frequencies	# freqs / decade	min frequency	max frequency	Version code
01_Nov26	70	70	2.167	20	3	n	3%	10%	-	0.03	0.2	50000	n	0	62	67	114	150	25	100	49	13	3	0.03	300	1.1.6
02_Dec27	20	20	3.132	20	10	n	3%	10%	-	0.03	0.1	10000	n	0	70	80	151	150	10	100	70	23	4	0.003	1000	1.1.6
03_Dec28	30	30	2.824	02_20iter	3	n	3%	10%	-	0.03	0.1	10000	n	0	70	80	151	150	10	100	70	23	4	0.003	1000	1.1.6
04_Jan22	15	15	2.972	20	10	n	3%	10%	-	0.03	0.1	10000	n	0	78	88	141	150	10	100	70	23	4	0.003	1000	1.1.6
05_Jan23	20	35	2.404	04_15iter	3	n	3%	10%	-	0.03	0.1	10000	n	0	78	88	141	150	10	100	70	23	4	0.003	1000	1.1.6
06_Jan25	30	65	1.953	05_20iter	1	n	3%	10%	-	0.03	0.1	10000	n	0	78	88	141	150	10	100	70	23	4	0.003	1000	1.1.6
07_Mar02	10	10	3.219	20	0.05	n	3%	10%	-	0.03	0.1	10000	n	0	78	88	141	150	10	100	70	13	2	0.003	1000	1.1.6_3
08_Mar03	11	21	2.607	07_10iter	0.05	n	3%	10%	-	0.03	0.1	10000	n	0	78	88	141	150	10	100	70	23	4	0.003	1000	1.1.6_3
08_Mar04	**19**	**40**	**2.119**	**08_11iter**	**0.05**	**n**	**3%**	**10%**	**-**	**0.03**	**0.1**	**10000**	**n**	**0**	**78**	**88**	**141**	**150**	**10**	**100**	**70**	**23**	**4**	**0.003**	**1000**	**1.1.6_3**

The final model presented in this model is #08 in the list.

Cumulative iteration	Inversions involving a re-start (typically with lower tau, see below): total number of iteration considering also the number of previous iterations.
Rms	Root mean square: measure of data fit (see also glossary in Appendix E). Average number of standard deviation between the model data and the observed data
Tau	Regularization parameter that controls the tradeoff between fitting the data and adhering to the model constraint (larger values cause a smoother model at the expense of a worse data fit)
lnZxy amplitude (& phase), Zxx/Zyy	Error floors in % (absolute for tipper). Please not that logarithm has been calculated in the xy and yx cases
Regularization	Regularization operator measuring the model structure/roughness
Tau (m-m0)	Constraint penalizing any deviations from the a-priori model, contributing to the total objective function.
Min, max resistivity	Resistivity bounds used in inversion.
nx, ny, nz	number of cells in the x, y, z direction
min dx, min dy, min dz	minimum cell dimension in the x, y, z direction (in meters)
Alpha	Regularization weight in x, y, and z directions. Higher values result in rougher model structure / more smoothing in the respective direction.

APPENDIX D DIGITAL DATA

D.1 CONTENT ON CD

The enclosed CD contains:

WinGLink Database

WinGLink database, with all MT data and 3D inversion results.

Report

Alum-SilverPeak_FinalReport.pdf: Acrobat pdf file of this report.

Plates and Resistivity Cross Sections from 3D MT inversion (see Appendix E)

3D Inversion Results

The 3D model mesh, the inversion statistics, the RMS misfit file and the predicted MT response files at each site (EDI files) are as follows:

D.2 OUTPUT DATA FORMATS

Inversions are distinguished by project name and model run number. The files associated with the 3D inversions consist of the following:

- model file (model_3dmod.out), which contains the mesh specifications and the final resistivity values;
- model.log, which contains inversion statistics;
- model.rms, in which the rms misfit for each station is listed;
- predicted data, in EDI format, that is, the computed impedance responses at each site.

D.2.1 MODEL FILE

This is an ASCII fixed-format file, which begins in the following form:

```
   72      94      122      13  VAL
11917    8512     6080     4343     3102
 2216    1583     1131      808      577
  412     294      210      150      150
  150     150      150      150      150
  150     150      150      150      150
    1 …
```

In this, the first three figures indicate the number of cells in the x, y, and z directions, and the following three rows list the cell dimensions in meters. The number 1 (fourth row) is a flag indicating that the resistivity values follow, and these are listed in the order of row (x), horizontal column (y), and depth (z) respectively.

At the end of the file, five lines contain the information needed to locate the mesh on the real world coordinate system. Here an example from the Alum model files.

```
WINGLINK
 Site_not_set      (site name)
        1          1    (i j block numbers)
384.74400862   4185.1498780     (real world coordinates)
           58    (rotation)
         1.82    (top elevation)
```

The model cell for reference purposes is indicated on the first line, with its coordinates (i, j) relative to the 3D mesh (of which cell 1,1 is in the extreme north-west). The following line gives the coordinates of the centre point of this cell in kilometres on the local reference system (here: UTM zone 11N, NAD83).

D.2.2 PREDICTED DATA

The computed responses are output in separate EDI files (Wight, 1988), one per site. These contain the frequencies and computed impedances corresponding to the final 3D inversion model.

D.2.3 INVERSION LOG AND ERROR FILE

File .log lists the inversion parameters, and, for each iteration, the rms misfit and objective functions. File .rms lists the final rms misfit between the observed and computed responses at each station.

APPENDIX E PLATES AND CROSS-SECTIONS

E.1 RESISTIVITY DEPTH MAPS

MT station and profile locations are shown on topographic base map in Plate 1.

The 3D resistivity mesh is illustrated via 10 depth slice maps, Plate Alum-2a-j, on a 1:50,000 scale and Plate SilverPeak-2a-j, on a 1:45,000 scale.

The resistivity colour scale is identical for all the resistivity maps.

E.2 RESISTIVITY CROSS-SECTIONS

Resistivity cross-sections from 3D MT inversion are plotted for profile A-1 to A-7 for Alum area, and for profiles SP-1 to SP-10 for Silver Peak area. Horizontal and vertical scales are at 1:30,000, respectively (vertical exaggeration is 1).

The resistivity colour scale is identical for all the resistivity cross-sections.